DOI: 10.1021/ma901365c

Macromolecules
ARTICLE

Fabrication of Poly(vinylidene fluoride−trifluoroethylene)/Poly(3,4-ethylenedioxythiophene)−Polystyrene Sulfonate Composite Nanofibers via Electrospinning

Osmarie Martínez,[†] Ariana G. Bravo,[†] and Nicholas J. Pinto*[,‡]

[†]*Department of Biology and* [‡]*Department of Physics and Electronics, University of Puerto Rico-Humacao, Humacao, PR 00791*

Received June 25, 2009; Revised Manuscript Received August 14, 2009

ABSTRACT: Nanofibers of PVF_2−TrFE/PEDOT−PSS were fabricated at room temperature using electrospinning with the thinnest fiber having a diameter of ∼15 nm. This process for generating PVF_2−TrFE/PEDOT−PSS composite nanofibers is cheap, fast, and reliable. The presence of conducting PEDOT−PSS assisted in the fabrication of PVF_2−TrFE nanofibers at low polymer concentrations in *N*,*N*,-dimethylformamide and energy dispersive X-ray spectroscopy confirmed the presence of PEDOT−PSS in the nanofibers. As a fiber mat, they were electrically conducting and used in the fabrication of a Schottky diode, and the diode parameters were calculated assuming the standard thermionic emission model of a Schottky junction. Being a composite, these nanofibers are promising candidates for use in a variety of applications that can take advantage of the ferroelectric and/or conducting properties of each individual component. In addition, the large aspect ratio and even larger surface to volume ratio of the fibers makes them ideal candidates in the fabrication of miniaturized, low power consumption devices, and supersensitive sensors.

Introduction

The electrically insulating polymer, poly(vinylidene fluoride) ($-CF_2-CH_2-$) (PVF_2) and some of its copolymers with trifluoroethylene ($-CF_2-CHF-$) (TrFE) are known to exhibit ferroelectric behavior.[1−7] While PVF_2 can exist in several different forms, not all of which are polar, the copolymer poly(vinylidene fluoride−trifluoroethylene), $(-CF_2-CH_2-)_n-(CF_2-CHF-)_m$ (PVF_2−TrFE) is polar for TrFE content in the range 20−50% at room temperature[3] and consists of an all trans configuration as shown in Figure 1a. The bistable nature of the permanent electrical dipoles that point perpendicular to the polymer backbone are responsible for the observable macroscopic polarization and has been put to use in nonvolatile organic memory devices.[8−11] Such information storage devices, where the basic storage element is the metal/ferroelectric polymer/metal capacitor, have been fabricated using low cost solution processability usually via spin coating techniques that lead to thin film based devices and are two-dimensional (2D) in nature. More recently, ferroelectric polymers have also been employed as the gate dielectric in the fabrication of ferroelectric field effect transistors (FeFET), where the polarization of the ferroelectric via a gate voltage controls the charge transport across a semiconducting channel in intimate contact with the gate dielectric.[12−14]

Conducting polymers, on the other hand, also form another class of technologically important organic materials whose applications range from corrosion prevention of metals[15] to more complex uses in organic field effect transistors[16−18] and other optoelectronic devices.[19,20] Unique to conducting polymers is the concept of doping, where the conductivity of the polymer can be varied controllably and reversibly without degradation, by several orders of magnitude[21] from the insulating to the conducting state and vice versa, a feature not possible in traditional metals. While doped polyaniline has aroused wide scientific interest, the conducting polymer poly(3,4-ethylenedioxthiophene)−PEDOT is technologically more desirable and hence has been used in most polymer based electronic applications. One of the reasons is that PEDOT is very stable in the doped state with conducting properties that remain unchanged with time under ambient environmental conditions.[22] Using a water-soluble polyelectrolyte (polystyrene sulfonic acid) (PSS), the commercially available PEDOT−PSS is also very stable in air and is water soluble. Figure 1b shows the chemical structure of this polymer which is sold commercially as a 1.3% w/w (∼1:2.5 PEDOT−PSS; doping level of ∼1/3 ethylenedioxythiophene) in water by Bayer Corp.[23]

Combinations of ferroelectric polymers (FP) and conducting polymers (CP) have been used in the fabrication of hybrid inorganic/organic or all polymer based devices.[13] Typically, these device architectures utilize the conducting polymer primarily as the electrical interconnects or electrodes and the ferroelectric polymer as the electroactive element, for example, in bimorphs[24] or in some cases the FP is the gate dielectric and the CP is the active element as in field effect transistors.[13] Combining ferroelectric and conducting polymers in the form of blends or composites can lead to new functional materials that could profit from the mechanical, electrical, and optical properties of the individual components. Most experimental work done in the past were carried out on thin films fabricated either via spin coating or electrochemical polymerization on planar substrates and are 2D.[25] In this paper, we present the first report on the fabrication of long (several millimeters) PVF_2−TrFE/PEDOT−PSS composite nanofibers via electrospinning. The concentration of the PEDOT−PSS is kept small in order to have a uniform homogeneous solution with no phase separation. Since most devices based on FP/CP materials utilize thin films, the relative ease in fiber preparation of these composites, as outlined in this paper, opens up the range of applications where the high aspect ratio and large surface to volume ratio of the fibers can be exploited in the

*To whom correspondence should be addressed. E-mail: nicholas.pinto@upr.edu.

 Published on Web 09/04/2009

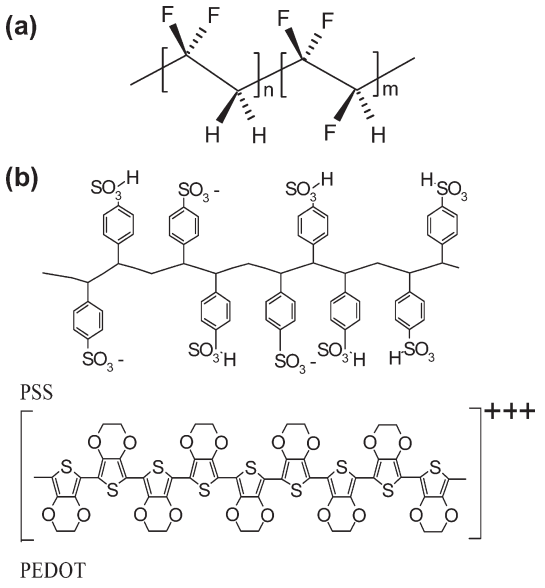

Figure 1. (a) Chemical structure of poly(vinylidene fluoride−trifluoroethylene), $(-CF_2-CH_2-)_n-(CF_2-CHF-)_m$, PVF_2-TrFE. (b) Chemical structure of poly(3,4-ethylenedioxthiophene)−poly(styrene sulfonate), PEDOT−PSS.

fabrication of quasi 1D low power consumption devices and supersensitive sensors. The fibers were characterized using several surface science characterization techniques and the electrical conducting properties of these fibers were put to use in the fabrication and testing of a Schottky diode.

Experimental Section

Chemicals. PVF_2-TrFE (75/25) purchased from Kureha, Japan (KF W no. 2200) was 99.9% pure and was used as received. The polymer molecular weight was 350 000 and was soluble in *N*,*N*,-dimethylformamide (DMF). In this work, the following concentrations of PVF_2-TrFE in DMF were prepared: 13, 10, 7, 5, and 3 wt %. For future reference, each of these solutions is designated as part A.

PEDOT−PSS was purchased from Bayer Corp. (Baytron P) and used as received. This Bayer product has a 1.3 wt % of the polymer in water. Prior to use, the PEDOT−PSS aqueous solution was filtered using a 0.45 μm PTFE syringe filter. For future reference, this solution is designated as part B.

The two parts prepared above were mixed in the following fixed mass ratio for each of the samples studied: 0.85 g of part A and 0.11 g of part B were mixed slowly in a 20 mL glass vial until the resulting solution was uniform and homogeneous with no solid residues. Thus for example, a sample labeled as 13 wt % PVF_2-TrFE/PEDOT−PSS for electrospinning was prepared by mixing 0.85 g of the 13 wt % PVF_2-TrFE/DMF solution with 0.11 g of the PEDOT−PSS water solution. The solid polymer PEDOT−PSS mass to that of PVF_2-TrFE was calculated to be 1.3, 1.6, 2.3, 3.2, and 5.3% for the 13 wt % PVF_2-TrFE/PEDOT−PSS, 10 wt % PVF_2-TrFE/PEDOT−PSS, 7 wt % PVF_2-TrFE/PEDOT−PSS, 5 wt % PVF_2-TrFE/PEDOT−PSS and 3 wt % PVF_2-TrFE/PEDOT−PSS solutions, respectively. The concentration of PEDOT−PSS is kept constant in all the samples even though the concentrations of PVF_2-TrFE are different. The final solution will therefore have a smaller PVF_2-TrFE concentration. Further addition of part B to increase the PEDOT−PSS concentration in any of the solutions prepared above resulted in the precipitation of PVF_2-TrFE at room temperature. Solutions using one-third lesser amount of part B (0.037 g) with part A held fixed at 0.85 g were also prepared.

Nanofiber Fabrication. Although discovered in the first half of the 1900s,[26,27] electrospinning is increasingly becoming very popular in several research laboratories worldwide in the preparation of polymer fibers either in the isolated form or nonwoven fiber mats.[28−30] Figure 2 shows the basic elements of the electrospinning apparatus used in this work and consists of a hypodermic syringe (1/2 cc tuberculin syringe), a high voltage power supply (Gamma Research), a grounded cathode (Al foil), and a syringe pump (Cole Parmer). About 0.5 mL of the appropriate solution prepared as indicated above was placed in the hypodermic syringe and the needle connected to the power supply with the cathode grounded and situated about 20 cm from the tip of the needle. The flow rate was controlled so that a drop fell out from the needle every 20 s. As the voltage applied to the needle is increased to about 8−10 kV, the electric force on the polymer droplet at the end of the needle overcomes the surface tension and a jet is issued forth in the form of a very fine spiral. Then, as the solvent evaporates, fibers of the polymer are seen to collect on the cathode. If allowed to continue for several minutes, a free-standing nonwoven fiber mat can be peeled off the Al foil. Individual fibers can also be captured by passing a polished Si/SiO_2 wafer perpendicular to the path of the jet in a downward sweeping action. The fibers land on the substrate and adhere to it, most likely due to interactions between PEDOT:PSS−SiO_2, where charged PEDOT:PSS can interact with possible silanol, Si−OH, groups on the SiO_2 surface. All of the fiber samples were dried in air at 100 °C for 30 min before surface characterization and for 24 h before electrical characterization.

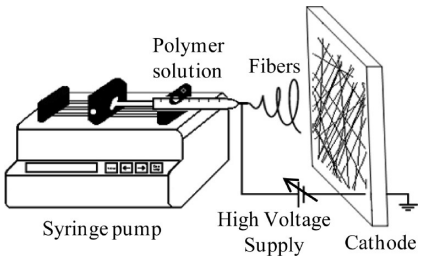

Figure 2. Schematic of the basic electrospinning apparatus. The syringe pump was programmed to result in a flow of one drop per 20 s to exit the needle.

Nanofiber Characterization. A Nikon Eclipse ME300 optical microscope fitted with a Sony DKC 5000 digital camera was used for optical images of the fibers. A JEOL JSM-6360 scanning electron microscope (SEM) with energy dispersive X-ray spectra microanalysis (EDS) capabilities was used to observe the fiber morphology at higher magnification and determine part of its chemical composition. The fiber diameter was determined using an Alpha Step 500 surface profiler (KLA Tencor) on individual fibers captured on polished Si/SiO_2 substrates. UV/vis spectra were obtained from polymer solutions before electrospinning using a Perkin-Elmer Lambda 35 spectrometer. Electrical characterization was performed on a fiber mat captured on prepatterened n-doped Si/SiO_2 substrates using a Keithley Model 6517A electrometer in a vacuum of 10^{-2} Torr to avoid any effects of moisture.

Results and Discussion

UV/vis Characterization. Figure 3 shows the UV/vis spectra of the solutions prepared from various PVF_2-TrFE concentrations with PEDOT−PSS. From this figure we see that when compared to the spectrum of pure PEDOT−PSS, regardless of the PVF_2-TrFE concentrations in solution, all of the UV/vis absorption spectra (except for the pure PVF_2-TrFE spectra) exhibit a relatively sharp UV absorption in the range 350−450 nm and an intense and broad absorption starting at larger wavelengths of about ~700 nm. The high energy transition is assigned to the n−π* transition in the PEDOT backbone and the broader transition represents the free carrier tail that is common to conducting

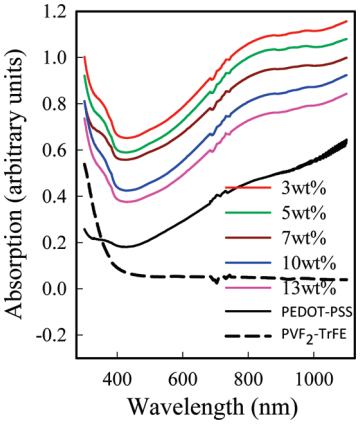

Figure 3. UV/vis spectra of the solutions prepared from various PVF_2−TrFE concentrations with PEDOT−PSS. Also included is the spectrum for pure PEDOT−PSS and PVF_2−TrFE. Individual traces have been shifted to avoid overlap.

polymers.[31] These results imply that the PEDOT−PSS is uniformly incorporated as a composite in the solution. Further observation that the solutions once prepared and stored in glass vials, stayed homogeneous for several weeks with no indication of phase separation of the PVF_2−TrFE/DMF and PEDOT−PSS water components strengthens the claim that the PEDOT−PSS is well dispersed in the PVF_2−TrFE/DMF solution.

Fiber Morphology. Figure 4 shows SEM images of the electrospun solutions of PVF_2−TrFE (3 and 5 wt %) with and without the presence of PEDOT−PSS. At such low concentrations, the break-up of the electrospun jet due to reduced extensional viscosity[32] prevents the formation of fibers as the solvent evaporates. The high boiling point of DMF also necessitates the use of a higher polymer concentration for fiber formation. In essence, what is observed is similar to a spraying effect that covers the cathode with tiny droplets and solid beads as was observed on the Al foil after termination of the electrospinning process. A small portion of the polymer deposited on the cathode could therefore have also been from dried liquid drops that lead the formation of thin films interdispersed with polymer beads due to electrospinning. A closer look at Figure 4c shows the very first faint appearances of extremely fine fibers emanating from some of the beads (spheres) and whose presence is certainly visible as the polymer concentrations increase, as seen in Figure 5a,c,e for the 7 wt % PVF_2−TrFE, 10 wt % PVF_2−TrFE, and 13 wt % PVF_2−TrFE samples, respectively. Increasing the solution viscosity by increasing the polymer concentration leads to the facile formation of fibers albeit with larger diameter and is clearly seen in Figures 5a,c,e. No liquid droplets were seen to accumulate on the cathode in electrospun polymer concentrations larger than 5 wt %. Above 10 wt %, the fiber morphology is markedly different. All of the beads which are mostly spindlelike are connected primarily by two fibers at diametrically opposite ends, and a single fiber could have several beads along its length.

The nonuniformity, short lengths and scant number of PVF_2−TrFE fibers, as seen in Figures 4a,c and Figures 5a,c, make them impractical for use in devices and sensors. In the electrospinning process it is known that the net charge density in the electrospinning jet and reduced surface tension lead to uniform fibers without beads. This could be accomplished by using an ionic salt (i.e., NaCl) to the solution.[28] We have chosen to increase the solution charge density by using a conducting polymer PEDOT−PSS. Thus, for example

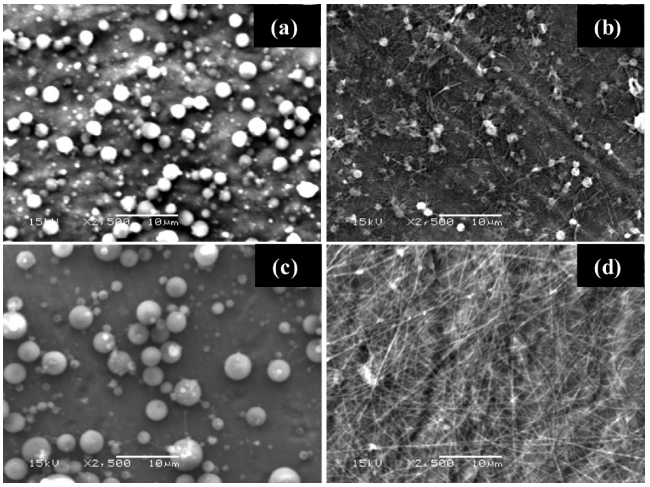

Figure 4. SEM images of electrospun fibers of (a) 3 wt % PVF_2−TrFE; (b) 3 wt % PVF_2−TrFE/PEDOT−PSS; (c) 5 wt % PVF_2−TrFE; and (d) 5 wt % PVF_2−TrFE/PEDOT−PSS. The magnification in all the images is the same and the scale bar is 10 μm.

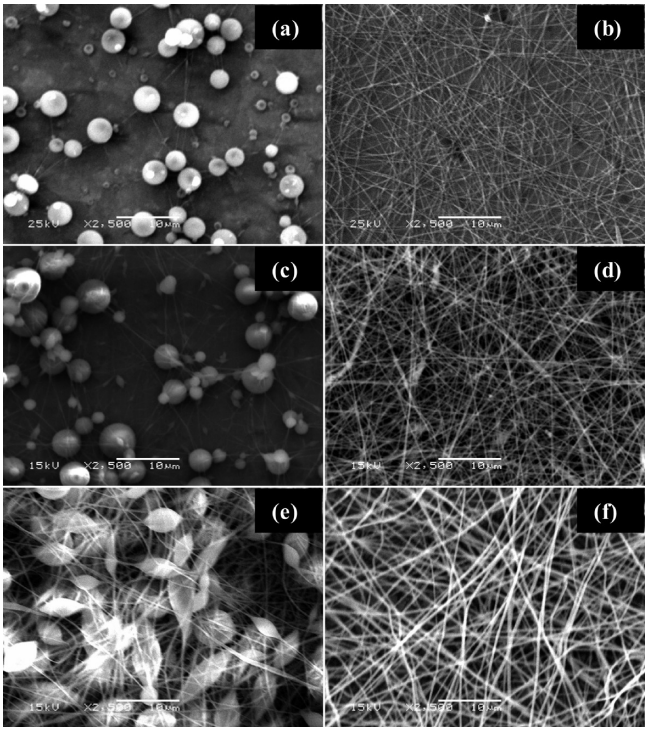

Figure 5. SEM images of electrospun fibers of (a) 7 wt % PVF_2−TrFE; (b) 7 wt % PVF_2−TrFE/PEDOT−PSS; (c) 10 wt % PVF_2−TrFE; (d) 10 wt % PVF_2−TrFE/PEDOT−PSS; (e) 13 wt % PVF_2−TrFE; and (f) 13 wt % PVF_2−TrFE/PEDOT−PSS. The magnification in all the images is the same and the scale bar is 10 μm.

in Figure 4b,d the presence of PEDOT−PSS leads to the formation of fibers, where without it there were practically none. Figure 5b,d,f also shows that PEDOT−PSS actively assists in the formation of nanofibers without the beading effect and by being present in the fiber. The role of the PEDOT−PSS in the electrospinning process is therefore two-fold, (i) facilitate the formation of PVF_2−TrFE nanofibers from dilute polymer solutions in DMF and (ii) retain the conducting properties in the composite nanofibers thereby increasing the potential functionality of the nanofiber. The fibers formed were long (several millimeters) and were physically seen to grow longer and directed toward the

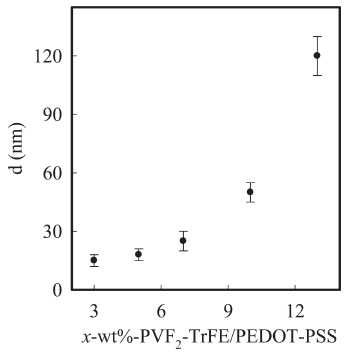

Figure 6. Graph of the diameters (d) versus weight concentrations of PVF_2−TrFE/PEDOT−PSS samples studied. The diameters were extracted from the vertical step height of the profilometer scan.

needle tip (once one end was anchored to the cathode) as free-standing "webs" suspended in air between the cathode and the tip of the needle, especially for the 13 wt % PVF_2−TrFE/PEDOT−PSS solution. The free-standing webs had to be physically removed in order to allow for the continuous formation of nanofibers. We have also seen that adding one-third lesser amount of PEDOT−PSS to the 5, 7, 10, and 13 wt % PVF_2−TrFE/DMF solutions also leads to uniform fibers with practically no beads.

Fiber Diameter. Individual fibers captured on polished Si/SiO_2 wafers were placed in the profilometer stage and scanned. Figure 6 shows the fiber diameter as a function of wt % PVF_2−TrFE/PEDOT−PSS for each of the different samples studied. The fiber diameters were 15, 18, 25, 50, and 120 nm for the 3 wt % PVF_2−TrFE/PEDOT−PSS, 5 wt % PVF_2−TrFE/PEDOT−PSS, 7 wt % PVF_2−TrFE/PEDOT−PSS, 10 wt % PVF_2−TrFE/PEDOT−PSS, and 13 wt % PVF_2−TrFE/PEDOT−PSS samples, respectively. This is consistent when one carefully observes the SEM images of Figure 4b,d and Figures 5b,d,f where there appears to be a gradual increase in the fiber diameter. The more viscous 13 wt % PVF_2−TrFE/PEDOT−PSS solution has the largest diameter and the least viscous 3 wt % PVF_2−TrFE/PEDOT−PSS solution has the smallest. Fabrication of such thin nanofibers of PVF_2−TrFE/PEDOT−PSS composites have not been reported before and have the potential to lead to new applications where size, sensitivity, and a combination of ferroelectric and/or conducting properties are important considerations.

Electrical Characterization. The PVF_2−TrFE/PEDOT−PSS composites have the potential to be used in applications that take the advantage of the ferroelectric nature, the electrical conducting nature or both of the nanofibers. For dc conduction, it is necessary that charge flow from one electrode to the other. The PEDOT−PSS concentration must therefore be above some minimum threshold so that a continuous conducting path is present across the fiber. Given the hydrophobicity/hydrophilicity of the PVF_2−TrFE/PEDOT−PSS polymers, one way to test the continuity of PEDOT−PSS in the nanofiber is to fabricate devices and characterize them using dc voltages. Initial observations of the Al foil after electrospinning showed that for the 3 and 5 wt % PVF_2−TrFE/PEDOT−PSS the fiber deposits appeared slightly bluish, while for higher concentrations it appeared white. Figure 7 shows the EDS spectra of the electrospun nanofibers for the 3, 5, and 7 wt % PVF_2−TrFE/PEDOT−PSS solutions together with the spectra of pure PVF_2−TrFE and PEDOT−PSS. The presence of C and F in pure PVF_2−TrFE and the presence of C, O, and S in PEDOT−PSS is consistent with the chemical structure as

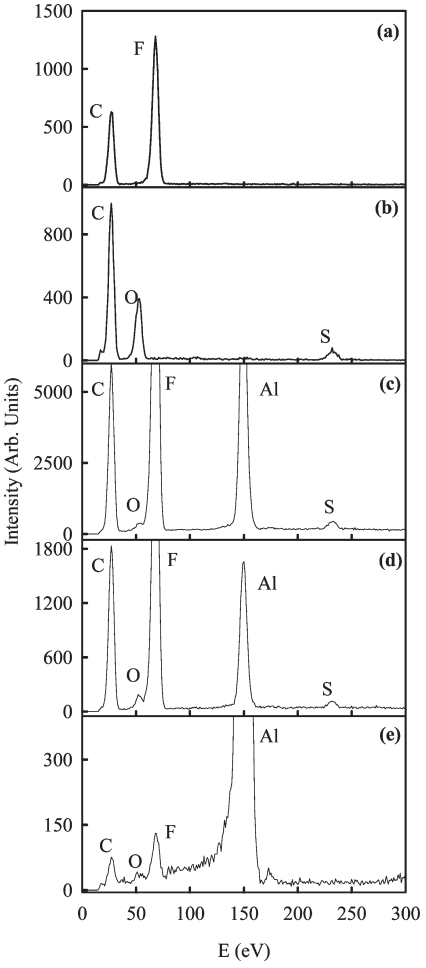

Figure 7. EDS taken from the SEM images for the following samples: (a) pure PVF_2−TrFE; (b) pure PEDOT−PSS; (c) 3 wt % PVF_2−TrFE/PEDOT−PSS; (d) 5 wt % PVF_2−TrFE/PEDOT−PSS; and (e) 7 wt % PVF_2−TrFE/PEDOT−PSS. The vertical scale in panels c, d, and e have been expanded to magnify the weak O and S signals. The Al signal is the aluminum substrate.

given in Figure 1. Even though the carbon and fluorine peaks appear to dominate the spectra in Figure 7c,d,e, nevertheless the oxygen and sulfur peaks are still discernible. For the 3, 5, and 7 wt % PVF_2−TrFE/PEDOT−PSS, the presence of all the atoms is indicative of the incorporation of PEDOT−PSS into the nanofibers. The Al peak appears as the substrate was made of aluminum foil. No evidence of O or S was seen for the samples of higher PVF_2−TrFE concentrations. One of the reasons could be the smaller amount of PEDOT−PSS relative to PVF_2−TrFE. However, the absence of beads in the electrospun fibers of these high concentration solutions suggests that a small fraction of PEDOT−PSS must be incorporated into the nanofibers.

Figure 8 shows the dc current−voltage (I−V) characteristics of several fibers prepared from the 5 wt % PVF_2−TrFE/PEDOT−PSS solution and deposited in the form of a fiber mat on a prepatterned n-doped Si/SiO_2 wafer. The top view optical image of the device is shown in the inset to Figure 8. A linear I−V response implies an ohmic contact of the fibers with the gold electrodes and the device conductance was 20 μS. Several devices were tested with electrode spacing ranging from 10 μm to several hundreds of micrometers and all were seen to allow a measurable flow of current under a ±1 V applied bias. A back gate bias did not affect the fiber mat conductivity which is reasonable

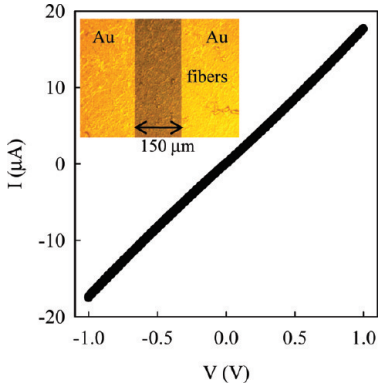

Figure 8. Current−voltage characteristics of a 5 wt % PVF_2−TrFE/PEDOT−PSS nanofiber mat electrospun across two gold leads taken at room temperature in vacuum. Inset: optical microscope image of the device.

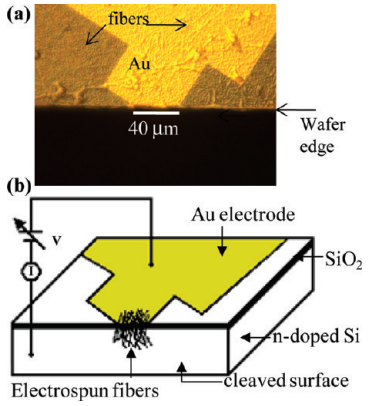

Figure 9. (a) Top view optical microscope image of the prepatterned n-doped Si/SiO_2 substrate cleaved through a gold electrode and covered with electrospun 5 wt % PVF_2−TrFE/PEDOT−PSS nanofibers. Many fibers reach over the edge making contact to the doped Si below the oxide layer. (b) Schematic of the optical image above with the external electrical connections.

given that PEDOT−PSS is a heavily doped conducting polymer. The conductivity of individual nanofibers was too small to be measured with the electrometer for any of the samples studied here. Given the reduced cross-sectional area of individual nanofibers and small percentage of PEDOT−PSS in the composite, this result is not surprising as any defects along the fiber length would restrict charge transport.

While individual fibers did not appear to conduct a current, the fiber mat was conducting, and the simplest device to fabricate and test using these fibers was the organic/inorganic Schottky diode. This is a two terminal device and consists of a junction of a p-doped polymer with an n-doped inorganic semiconductor. The Schottky diode was prepared by using an n-doped Si wafer (⟨111⟩, 0.1−1.0 Ω cm) with a 200 nm thermally grown oxide layer and 5 wt % PVF_2−TrFE/PEDOT−PSS. After prepatterning gold electrodes over the oxide via standard lithography and lift-off techniques, the substrate was cleaved through the electrodes. The exposed cleaved surface has the edge of the gold electrode separated from the doped Si by the insulating oxide layer. The cleaved substrate was placed on the Al foil during the electrospinning process and covered with nanofibers, many of which were long enough and crossed over the wafer edge making contact to the Au electrode above and to the doped Si below the oxide layer. The resulting Schottky diode was formed along the vertical edge of the substrate at the

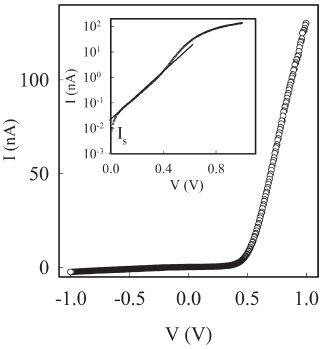

Figure 10. Current−voltage characteristics at 300 K of the Schottky diode shown in the previous figure. Inset: semilog plot of the forward bias current as a function of forward bias voltage. The linear intercept with the current axis at zero voltage represents the saturation current (I_s).

nanofiber-doped Si interface.[30] Figure 9a shows the top view optical image of the device where the cleaved section cuts through a gold electrode and several fibers are seen to reach over the wafer edge. Figure 9b shows the device schematic with the external electrical connections. Figure 10 shows the $I-V$ characteristic curve at 300 K of the device in vacuum. Since the fibers make ohmic contacts with Au electrodes, the nonlinear response arises from the Schottky barrier at the polymer-n-doped Si substrate. Under thermal equilibrium conditions with no applied external bias to the diode, the Fermi levels of the doped Si and that of PEDOT−PSS in the fiber mat must be coincident leading to band bending at the junction via the flow of charge from the semiconductor into the polymer setting up the Schottky barrier. PEDOT−PSS is known to have a band gap of about ∼1.6 eV.[22] Assuming that the band gap in the n-doped Si is ∼1.2 eV the corresponding schematic band diagram of the relevant energy levels at the polymer nanofiber/n-Si interface are shown in Figure 11, before and after physical contact. This band bending creates a space charge region resulting in a barrier to charge flow at the interface of the nanofiber and the semiconductor. For typical Schottky diodes, charge flow is via thermionic emission over the barrier and generally, the barrier height is determined by factors such as the polymer work function and the surface states on the semiconductor.[33] These devices exhibited rectifying behavior and the ratio of the forward to reverse current at a bias voltage of ± 1V for this device was calculated to be ∼50 and was limited in part due to the low fiber conductivity and the series resistance of the bulk semiconductor. The turn-on voltage obtained by extrapolating the current in the linear region ($V > 0.6$ V) to the voltage axis at zero current in Figure 10 was in the range 0.5−0.6 V.

In order to quantitatively analyze the diode characteristics, we assume the standard thermionic emission model of a Schottky junction as follows[34]

$$J = J_s\left[\exp\left(\frac{qV}{nkT}\right) - 1\right] \quad (1)$$

$$J_s = A^*T^2 \exp\left(-\frac{q\varphi_B}{kT}\right) \quad (2)$$

where J is the current density, J_s is the saturation current density, q is the electron charge, k is the Boltzmann constant, T is the absolute temperature, ϕ_B is the barrier height, and n is

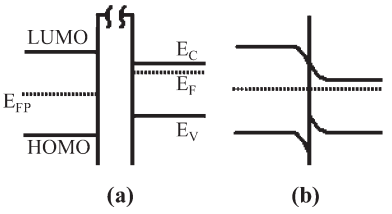

Figure 11. Schematic energy band diagrams for the formation of the PEDOT−PSS/n-Si interface (a) before and (b) after contact. E_C and E_V are the conduction and valence band edge energies of the n-Si. E_F and E_{FP} are the Fermi energy levels of the n-Si and PEDOT−PSS respectively. The LUMO and HOMO levels for PEDOT−PSS are also indicated. After contact, band bending helps establish a constant Fermi energy level across the interface at thermal equilibrium resulting in a Schottky barrier.

the ideality factor which takes into account corrections to the original simple model, for example, image-force barrier lowering. The Richardson's constant ($A^* = (4\pi qm^*k^2)/h^3$) is calculated to be 120 A/K^2-cm^2 assuming m^* is the bare electron mass. Using the data in Figure 10, the inset to this figure shows a representative semilogarithmic plot of the diode current versus applied voltage under forward bias conditions. At low biases, a linear variation of the current is observed consistent with eq 1 while the deviation from linearity at higher bias voltages generally is related to ohmic losses due to the diode series resistance. Assuming a uniform single layer of 20 nm diameter fibers crossing over the edge in Figure 9a and extrapolating the linear portion of the semilog plot to the current axis at zero bias yields a saturation current density of 2.2×10^{-3} A/cm^2 and the diode ideality factor calculated from the slope of the linear portion of this plot as follows

$$n = \frac{q}{kT}\left(\frac{\partial V}{\partial \ln J}\right) \tag{3}$$

is $n \sim 7.2$. Using these equations, we calculate the barrier height of 0.58 eV. The high values ($n > 1$) of the ideality parameter have been attributed to several factors that include the recombination of holes and electrons in the depletion layer,[35] the presence of an interfacial layer, and interface states at the polymer−semiconductor interface[36] or even a tunneling process.[37] Since the silicon substrate was not vacuum cleaved, there exists a strong possibility of the presence of dangling Si bonds at the cleaved surface that could interact with the fiber leading to an interfacial layer. Pretreating the substrates with dilute nitric acid could reduce this effect. Finally, the low turn-on voltage is especially beneficial for polymer based electronics that currently operate under high biases.

Conclusions

Composite nanofibers of PVF_2−TrFE with PEDOT−PSS were successfully fabricated via electrospinning. The addition of PEDOT−PSS assists in fiber formation making it possible to electrospin uniform nanofibers of PVF_2−TrFE at low polymer concentrations in DMF and without the beading effect in PVF_2−TrFE solutions with high polymer concentrations. The incorporation of PEDOT−PSS into the nanofibers was verified via energy dispersive X-ray spectroscopy and by fabricating and testing devices based on these nanofibers. The electrospinning process for generating nanofibers is cheap, simple to operate, and can be used to fabricate resistors and diodes using PVF_2−TrFE/PEDOT−PSS composites in air and within seconds. Nanofibers of PVF_2−TrFE/PEDOT−PSS are promising candidates for use in a variety of applications that require the ferroelectric and/or conducting properties of the composite fibers. In addition, the large aspect ratio and even larger surface to volume ratio of the fibers makes them ideal candidates in the fabrication of miniaturized, low power consumption devices and supersensitive sensors.

Acknowledgment. This work was supported by NSF under grants DMR-RUI-0703544 and DMR-PREM-0353730. Partial support for A. Bravo and O. Martinez was provided by NIH-RISE.

References and Notes

(1) Yamada, T.; Kitayama, T. *J. Appl. Phys.* **1981**, *52*, 6859.
(2) Lovinger, A. J.; Davis, G. T.; Furukawa, T.; Broadhurst, M. G. *Macromolecules* **1982**, *15*, 323.
(3) Lovinger, A. J.; Furukawa, T.; Davis, G. T.; Broadhurst, M. G. *Polymer* **1983**, *24*, 1225.
(4) Koizumi, N.; Haikawa, N.; Habuka, H. *Ferroelectrics* **1984**, *57*, 99.
(5) Bune, A. V.; Fridkin, V. M.; Verkhovskaya, K. A.; Taylor, G. *Polymer J.* **1990**, *22*, 7.
(6) Legrand, J. F. *Ferroelectrics* **1989**, *91*, 303.
(7) Moreira, R. L.; Gregoire-Saint, P.; Lopez, M.; Latour, M. *J. Polym. Sci., Part B: Polym. Phys.* **1989**, *27*, 709.
(8) Reece, T. J.; Ducharme, S.; Sorokin, A. V.; Poulsen, M. *Appl. Phys. Lett.* **2003**, *82*, 142.
(9) Lim, S. H.; Rastogi, A. C.; Desu, S. B. *J. Appl. Phys.* **2004**, *96*, 5673.
(10) Schroeder, R.; Majewski, L. A.; Voigt, M.; Grell, M. *IEEE Electron Device Lett.* **2005**, *26*, 69.
(11) Park, Y. J.; Kang, S. J.; Lotz, B.; Brinkmann, M.; Thierry, A.; Kim, K. J.; Park, C. *Macromolecules* **2008**, *41*, 8648.
(12) Naber, R. C. G.; Tanase, C.; Blom, P. W. M.; Gelinck, G. H.; Marsman, A. W.; Touwslager, F. J.; Setayesh, S.; De Leeuw, D. M. *Nat. Mater.* **2005**, *4*, 243.
(13) Gelinck, G. H.; Marsman, A. W.; Touwslaer, F. J.; Setayesh, S.; de Leeuw, D. M.; Naber, R. C. G.; Blom, P. W. M. *Appl. Phys. Lett.* **2005**, *87*, 092903.
(14) Kang, S. J.; Park, Y. J.; Sung, J.; Jo, P. S.; Park, C.; Kim, K. J.; Cho, B. O. *Appl. Phys. Lett.* **2008**, *92*, 012921.
(15) Wessling, B. *Adv. Mater.* **1991**, *6*, 226.
(16) Gelinck, G. H.; Geuns, T. C. T.; de Leeuw, D. M. *Appl. Phys. Lett.* **2000**, *77*, 1487.
(17) Garnier, F.; Hajlaoui, R.; Yassar, A.; Srivastava, P. *Science* **1994**, *265*, 1684.
(18) Tsumura, A.; Koezuka, H.; Ando, T. *Appl. Phys. Lett.* **1986**, *49*, 1210.
(19) Sirringhaus, H.; Kawase, T.; Friend, R. H.; Shimoda, T.; Inbasekaran, M.; Wu, W.; Woo, E. P. *Science* **2000**, *290*, 2123.
(20) Burroughes, J. H.; Jones, C. A.; Friend, R. H. *Nature* **1998**, *335*, 137.
(21) MacDiarmid, A. G.; Chiang, J. C.; Huang, W.; Humphrey, B. D.; Somasiri, N. L. D. *Mol. Cryst. Liq. Cryst.* **1985**, *125*, 309.
(22) Pei, Q.; Zuccarello, G.; Ahlskog, M.; Inganas, O. *Polymer* **1994**, *35*, 1347.
(23) Groenendaal, L.; Jonas, F.; Freitag, D.; Pielartzik, H.; Reynolds, J. R. *Adv. Mater.* **2000**, *12*, 481.
(24) Polasnik, T. P.; Schmidt, V. H. *Proc. of SPIE* **2005**, *5759*, 114.
(25) Skotheim T. A.; Reynolds J. R. *Handbook of conducting polymers*, 3rd ed.; CRC Press, Taylor and Francis: Boca Raton, FL, 2007; Vol. *2*, Section II, and references therein.
(26) Morton, W. U.S. Patent 705,691, **1905**.
(27) Formhals, A. U.S. Patent 1,975,504, **1934**.
(28) Reneker, D. H.; Yarin, L. Y. *Polymer* **2008**, *49*, 2387.
(29) MacDiarmid, A. G.; Jones, W. E.; Norris, I. D.; J. Gao, J.; Johnson, A. T.; Pinto, N. J.; Hone, J.; Han, B.; Ho, F. K.; Okuzaki, H.; Llaguno, M. *Synth. Met.* **2001**, *119*, 27.
(30) Pinto, N. J.; González, R.; Johnson, A. T., Jr.; MacDiarmid, A. G. *Appl. Phys. Lett.* **2006**, *89*, 033505.
(31) Hohnholz, D.; MacDiarmid, A. G.; Sarno, D. M.; Jones, W. E., Jr. *Chem. Commun.* **2001**, 2444.
(32) Yu, J. H.; Fridrikh, S. V.; Rutledge, G. C. *Polymer* **2006**, *47*, 4789.
(33) Sze, S. M. *Physics of Semiconductor Devices*; Wiley: New York, 1981; Chapter 5, p 255.
(34) Horowitz, G. *Adv. Mater.* **1990**, *2*, 287.
(35) Gupta, R. K.; Singh, R. A. *J. Polym. Res.* **2004**, *11*, 269.
(36) Saglam, M.; Biber, M.; Cakar, M.; Turut, A. *Appl. Surf. Sci.* **2004**, *230*, 404.
(37) Halliday, D. P.; Gray, J. W.; Adams, P. N.; Monkman, A. P. *Synth. Met.* **1999**, *102*, 877.